22nd International Conference on Sustainable Energy Technologies
Kuala Lumpur, Malaysia, 13 to 15 August 2026 · ISBN 978-1-995850-00-9 · ISSN 2978-4387

CONFERENCE PAPER · ENERGY STORAGE & CONVERSION

Climatic Adaptability of Customized Phase Change Energy Piles Based on the Random Aggregate Method

Zhengheng Gan[1], Mei Yin[1]*, Shiqi Dou[2], Hu Fan[1], Chaokai Zhang[1]

[1] School of Civil Engineering, Southeast University, Nanjing 211189, China
[2] College of Civil Engineering, Tongji University, Shanghai 200092, China

RECEIVED 2 February 2026 · REVISED 7 March 2026 · ACCEPTED 20 March 2026
PRESENTED 13 to 15 August 2026 · PUBLISHED 23 November 2026

ABSTRACT

This study investigates the climatic adaptability of customised phase change energy piles by developing region-specific binary composite phase change materials (PCM) and employing a random aggregate method (RAM) for three-dimensional numerical modelling. Two binary eutectic PCM formulations were prepared via melt-blending: a capric acid/methyl stearate (CA/MS) composite with a phase transition temperature of 21.1 °C for warm regions, and a capric acid/methyl palmitate (CA/MP) composite at 17.2 °C for cold regions. The PCM were macro-encapsulated within hollow steel balls (HSB) and embedded as discrete inclusions within the concrete pile matrix. Unlike conventional homogenisation approaches, the proposed RAM explicitly models the heterogeneous spatial distribution of HSB-PCM particles, enabling the capture of local thermal responses and asynchronous phase change behaviour at the cross-sectional scale. A numerical model was established in COMSOL to evaluate the thermal performance of an energy pile under 10-day cyclic thermal loading. Results demonstrate that the depth-wise temperature difference within the pile converged from 0.490 °C (1st cycle) to 0.257 °C (10th cycle) for the warm-region (SPEP) and from 0.541 °C to 0.344 °C for the cold-region (PPEP), indicating progressive thermal stabilisation. The steady-state heat transfer efficiency of the SPEP decreased from 93.85 W/m to 81.30 W/m over 10 cycles (a cumulative decline of 13.4%). Research has found that the heat-affected zone of the pile is primarily confined to an area within twice the diameter of the pile. This study provides a theoretical basis and practical guidance for the regional application of HSB-PCM in energy pile engineering.

KEYWORDS Energy piles, Random aggregate method, Composite PCM, COMSOL simulation

1. Introduction

In the context of addressing global warming and the energy transition, shallow geothermal energy has become a key focus in the field of building energy efficiency due to its vast reserves and widespread distribution (Huang *et al.* 2026; Luu *et al.* 2025). As an innovative form that integrates structural load-bearing and heat exchange, energy piles enable the efficient extraction of geothermal energy through the installation of buried piping (Chang *et al.* 2025; Han and Yu 2020; Ng *et al.* 2015; Yang *et al.* 2025). However, during long-term operation in actual engineering projects, significant thermal accumulation or thermal deficit often occurs in the soil surrounding the piles due to seasonal thermal load imbalances (Chang *et al.* 2024; You and Zeng 2023). This thermal imbalance not only reduces the coefficient of performance (COP) of ground-source heat pump systems but may also induce thermal stress damage to the pile body, severely limiting the large-scale deployment of energy piles (Kong *et al.* 2019; Xia *et al.* 2021; Yin *et al.* 2025; You and Zeng 2023).

The integration of PCM into concrete is an effective strategy for addressing the aforementioned challenges (Chang *et al.* 2026a; Chen *et al.* 2025; Han *et al.* 2022). PCM utilise the high latent heat released during their phase change process (Song *et al.* 2019; Zhang *et al.* 2021) to act as a thermal

* Corresponding author. Email address: mei.yin@seu.edu.cn (Mei Yin)

© 2026 The Author(s).
Published by Caravel Press.

doi.org/10.65582/set.2026.002

buffer (absorbing heat during peak thermal loads to reduce temperature fluctuations), thereby significantly enhancing the thermal stability of pile foundations (Cao *et al.* 2022; Mousa *et al.* 2022; Reboli *et al.* 2025). However, existing research often overlooks the influence of regional climate on the performance of PCM. Previous studies have used grating sensors to monitor energy piles under different climatic conditions (Song *et al.* 2020). The results indicate that the stresses and irreversible displacements caused by thermal loads increase with the number of thermal cycles, providing a reference and basis for the design of energy piles in different climatic zones. Wu *et al.* (2019) conducted temperature cycling tests on friction piles and end-bearing piles under three different climate scenarios using a model testing approach. The results indicate that the irreversible displacement of friction piles is greater than that of end-bearing piles following thermal cycling. In climates dominated by low temperatures, energy piles exhibit the smallest thermally induced irreversible displacement. Morrone *et al.* (2014) conducted technical and economic analyses of heating and cooling scenarios by considering energy piles in conjunction with ground-source heat pump systems. At the same time, a 20-year numerical simulation of the ground-source heat pump was conducted to assess the system's long-term operational performance. It is crucial that the temperature range of the PCM matches that of the ground (Weng *et al.* 2025). In response to the differing requirements of cold and warm regions (Adebayo *et al.* 2024; Angrisani *et al.* 2016; Bourne-Webb and Bodas Freitas 2020; Ghezellou *et al.* 2024; Mu *et al.* 2026), this study proposes a region-specific development approach. In cold regions, formulations with low phase change points should be selected to facilitate heat extraction during winter, whilst in warm regions, formulations with high phase change points should be used to assist with heat dissipation during summer. By adjusting the composition ratios of binary eutectic mixtures, it is possible to precisely match the initial ground temperatures of different regions, thereby maximising the material's energy storage potential (Chang *et al.* 2026b).

In terms of thermal performance evaluation, the accuracy of numerical simulations directly determines the reliability of engineering designs. Current mainstream research predominantly employs the homogenisation assumption; however, this simplification overlooks the random distribution characteristics of PCM as a discrete phase within concrete (Hu *et al.* 2025; Yang *et al.* 2023). To objectively evaluate complex heat transfer in heterogeneous media, this study introduces the Random Aggregate Method (RAM). Among the simulation methods for PCM, the homogenisation model treats the PCM as a homogeneous continuous medium in which the components of each phase are distributed completely uniformly throughout the volume, whereas the random aggregate model distributes the PCM randomly within the matrix material in the form of discrete particles, thereby more closely approximating the actual microstructure (Chen *et al.* 2024; Gan *et al.* 2025). Homogenised models fail to capture non-uniform heat fluxes due to neglecting local thermal resistance, while random aggregate models account for local heat flux detours and accumulation caused by particle distribution. As a result, homogenised models are idealised and less physically realistic, while random aggregate models better represent heat transfer processes. Regarding phase changes, the homogenised model uses global averaging for latent heat but can't distinguish independent melting at different locations. In contrast, the random aggregate model simulates asynchronous melting by allowing each PCM particle to undergo phase change based on local temperature. Although computationally more complex, the random aggregate model offers superior thermodynamic accuracy, realism, and phase change representation.

This study developed two types of binary eutectic PCM for different climatic zones, integrating them into energy piles with macro-encapsulation technology. Using a three-dimensional numerical model based on the stochastic aggregate method, the phase change behaviour under heterogeneous constraints was investigated. The study experimentally validated the random distribution model's ability to capture local thermal responses and assessed the energy pile system's stability under long-term thermal cycling, providing theoretical and technical guidance for phase change energy pile applications in varying climates.

2. Materials and methods

The thermal extraction performance of the energy pile was improved using PCM. To ensure that the temperature characteristics of the PCM are suitable for different regions, two formulations of PCM were designed in this study.

2.1. Customized binary composite PCM preparation

Given the variations in ground temperatures across different regions, multi-component organic PCMs were selected to tailor the phase transition temperature to different climatic conditions. The binary PCMs were prepared using a melt-blending method based on binary eutectic systems and subsequently macro-encapsulated in hollow steel balls (HSBs), as shown in Figure 1. For warm regions, methyl stearate (MS) and capric acid (CA) were used to form the composite PCM, whereas capric acid (CA) and methyl palmitate (MP) were adopted for cold regions. The corresponding mass ratios and thermophysical properties of the two composite PCMs, including phase transition temperature, latent heat, density, thermal conductivity, and specific heat capacity, are summarised in Table 1. Material selection considered safety, latent heat storage capacity, and cost. These thermophysical properties were subsequently adopted as material inputs for the COMSOL simulations. In addition, the HSB macro-encapsulation configuration used in the material preparation was explicitly represented in the numerical model, where the PCM core and steel shell were treated as separate domains. Therefore, the material preparation and characterisation presented in this section provide the thermophysical and physical basis for the subsequent random aggregate modelling of HSB-PCM within the energy pile.

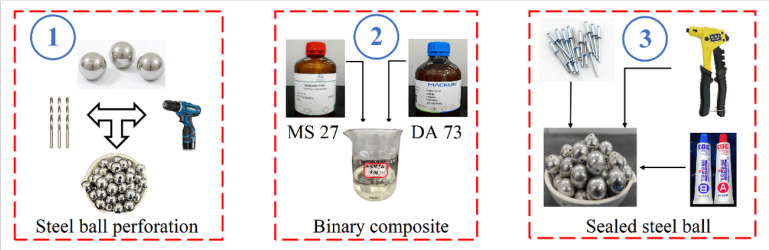

Figure 1. Phase change material mixing and packaging (Gan *et al.* 2025).

Table 1. Parameters of composite PCM.

Type	Composite system	Mass ratio	Phase transition temperature	Latent heat	Density	Heat transfer (solid/liquid)	Specific heat capacity
Hot	CA/MS	73:27	21.1	161.2	970	0.23/0.17	1973
Cold	CA/MP	47:53	17.2	173.8	895	0.2/0.18	2200

2.2. Numerical modelling methods

The model used in this study was created using COMSOL, with a pile length of 8 m and a pile diameter of 0.4 m. The heat exchange tube employs a single U-shaped configuration with an internal diameter of 20 mm. The foundation soil has a diameter of 10 m and a depth of 15 m, which ensures adequate coverage of the heat transfer region and accounts for boundary effects. Figure 2 illustrates the model mesh and the distribution of random phase change aggregates within the pile.

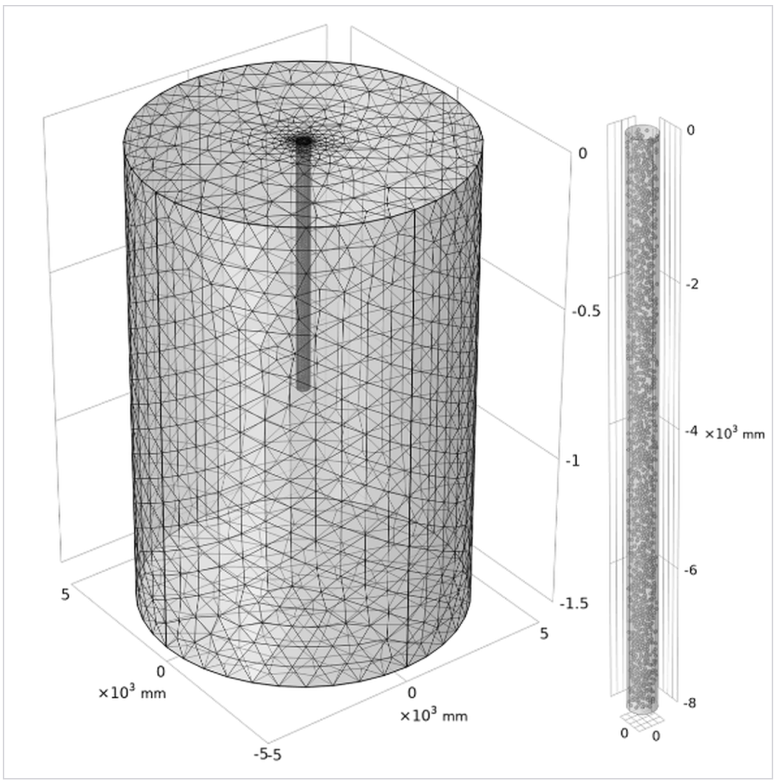

Figure 2. COMSOL model.

2.3. Random aggregate method

This study proposes a stochastic aggregate method to better represent the spatial distribution of PCM in energy piles. Unlike traditional studies that simplify modelling by assigning PCM thermal properties directly to the concrete, this homogenisation approach overlooks heterogeneous pile characteristics and local temperature variations. To address this, PCM is encapsulated within hollow steel balls, which are embedded as discrete inclusions in the concrete. The positions of the steel spheres are randomly generated to ensure a uniform distribution, avoiding artificial agglomeration and closely reflecting the actual material filling in engineering applications. The thermal properties of the PCM are assigned to the interior of the steel balls, while the surrounding concrete retains its properties, and the thermal conductivity of the steel shell is also considered. This heterogeneous approach allows for accurate temperature gradient analysis and captures thermal responses during local PCM phase changes. Compared to traditional models, the random aggregate method provides a more refined physical representation, improving the simulation of thermal responses and heat transfer in PCM energy piles. During model creation, the steel ball coordinates must satisfy four constraints: they must fit entirely within the pile body, maintain a centre-to-centre distance greater than 2r, stay at least r from the pile and heat exchange tube surfaces, and not deform or compromise pile integrity.

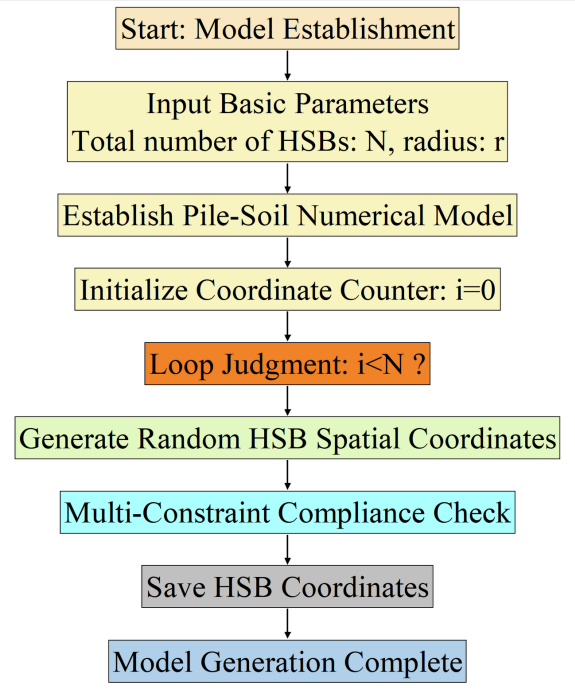

Figure 3. Random aggregate generation.

2.4. Parameters

Based on the above characteristics of physical field coupling, this study compares the thermal performance of phase change energy piles under different climatic conditions. The study investigates the thermal response of conventional piles, phase change piles in hot regions, and phase change piles in cold regions following a 10-day temperature cycle. The flow velocity in the heat exchange pipe is set at 0.6 m/s. The thermal properties used in the simulation are shown in Table 2.

Table 2. Model parameters.

Parameter	Unit	Value
Concrete density	kg/m³	2245
Thermal conductivity of concrete	W/(m·K)	1.426
Specific heat capacity of concrete	J/(kg·K)	928
Soil density	kg/m³	1860
Thermal conductivity of soil	W/(m·K)	1.3
Specific heat capacity of soil	J/(kg·K)	1300
Thermal conductivity of heat exchange tubes	W/(m·K)	0.4

2.5. Model validation

To ensure numerical accuracy, a mesh independence test was conducted before the main simulations. The model's accuracy was evaluated using the mean relative error (MRE) and root mean square error (RMSE). Figure 4(a) shows the temperature variation at measurement point T3 after 10 hours with progressively refined meshes (115054 to 216887 elements). Results converged as the mesh refined, and when the grid reached 151492 cells, the MRE between grids was just 0.21%, indicating negligible impact from further refinement. Thus, 151492 cells were selected for subsequent simulations.

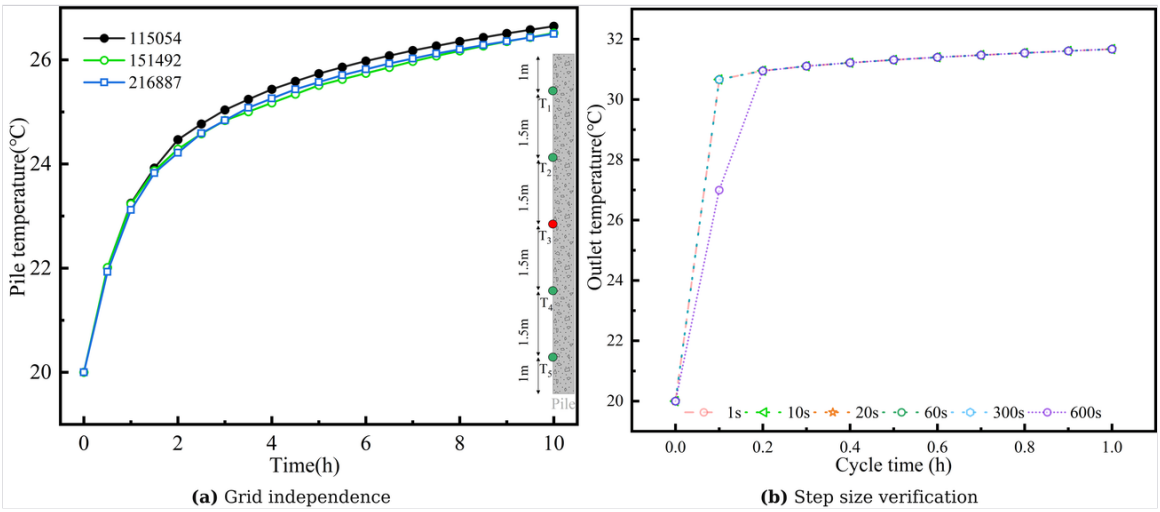

(a) Grid independence **(b)** Step size verification

Figure 4. Model verification.

A time-step independence test was also performed to assess temporal resolution. Figure 4(b) compares outlet temperature over time for different time steps (1 s, 10 s, 20 s, 60 s, 300 s, 600 s). For time steps ≤60 s, results were well-converged. However, larger time steps (≥300 s) caused deviations during the initial phase, particularly with the 600 s step, which underestimated outlet temperature. After 0.3 hours, results converged, indicating lower sensitivity to time step size once the system neared steady-state. A 60 s time step was chosen for its balance of accuracy and computational efficiency, suitable for large-scale parametric studies.

3. Results and discussion

3.1. Temperature distribution within the pile

Figure 5 illustrates that the temperature response of phase change energy piles (SPEP and PPEP) exhibits significant axial non-uniformity governed by the PCM's latent heat. During the heating phase (e.g., 10th cycle), the SPEP temperature increased with depth, peaking in the lower-middle section with a 0.257 °C gradient relative to the pile head. Notably, the depth-wise temperature difference converged from 0.490 °C (1st cycle) to 0.257 °C (10th cycle) for SPEP, and from 0.541 °C to 0.344 °C for PPEP, indicating the system evolves toward a steady state. During the natural recovery phase, temperature distribution became more uniform; the 10th cycle SPEP dropped by 5.692 °C (80% recovery), while PPEP rose by 5.326 °C (77% recovery). Interestingly, a gradient reversal occurred during recovery: SPEP decreased with depth while PPEP increased. This reversal stems from the greater thermal driving force in the middle-lower sections, which accumulate the most heat or cold during operation.

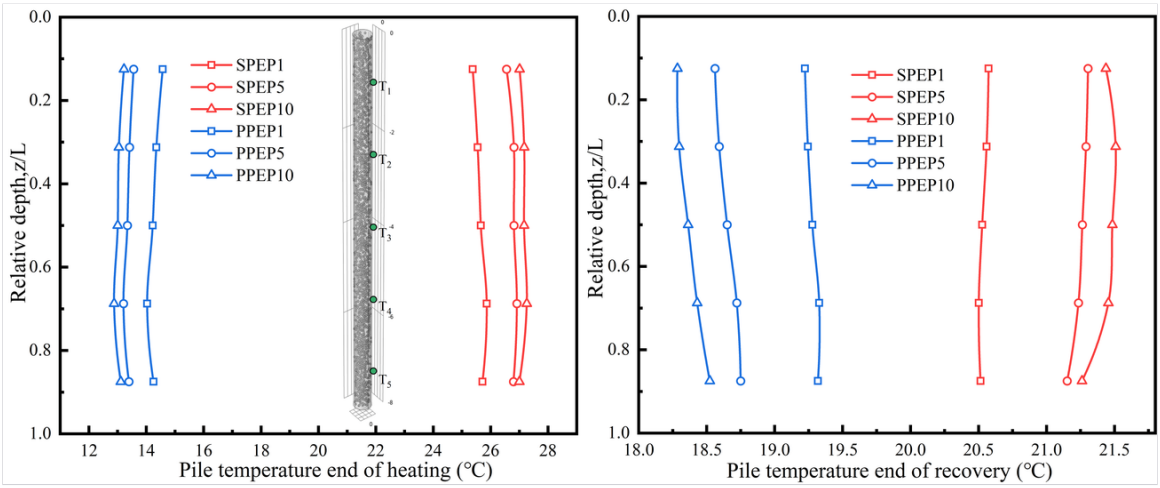

Figure 5. Pile temperature distribution with depth.

The cumulative cyclic effect shown in Figure 5 reveals a decaying trend in temperature drift. For SPEP, the average temperature rose by 1.145 °C over the first five cycles but only by 0.343 °C over the subsequent five; PPEP followed a similar decaying decrease. Recovery phase temperatures mirrored this, with SPEP rising by 0.893 °C and PPEP falling by 0.899 °C after 10 cycles. This 15–17% residual variation indicates that soil "residual heat" persists, influencing long-term efficiency. As depicted in Figure 5, the PCM effectively compresses the axial gradient to within 0.5 °C through its "peak-shaving" effect. Mechanistically, the pile ends reach equilibrium faster due to surface and toe boundary effects, whereas the middle-lower sections remain core heat exchange zones. Ultimately, the gradual drift of the surrounding soil temperature field dictates the monotonic yet converging evolution of the pile's thermal response toward a quasi-steady state.

Figure 6 shows the evolution of the temperature change ΔT in the pile body at measurement points T3 and T5 as a function of cycle time for SPEP and PPEP. The absolute peak temperature at each measurement point gradually increased with the number of cycles. Taking the T3 measurement point as an example, the peak ΔT for SPEP rose from 5.71 °C in the first cycle to 7.17 °C in the tenth cycle, representing a cumulative increase of 1.45 °C (25.4%). The absolute value of the cooling peak for PPEP increased from 5.78 °C to 7.00 °C, representing a cumulative increase of 1.22 °C (21.1%). However, the cyclic increments showed a significant decreasing trend; the peak increment for SPEP-T3 between the first and second cycles was 0.41 °C, having dropped to 0.05 °C in the final two cycles, with the first five cycles contributing over 85% of the total increment. This indicates that the heat exchange process within the pile-soil system is gradually approaching a dynamic equilibrium. Concurrently, following the recovery phase of each cycle, the pile temperature failed to return fully to its initial value, resulting in a continuously accumulating residual temperature. The residual temperature at the end of each cycle for SPEP-T3 gradually increased from 0.54 °C in the first cycle to 1.49 °C in the tenth cycle. For PPEP-T3, it evolved from −0.74 °C to −1.64 °C. The continuous accumulation of residual temperature indicates an irreversible shift in the thermal environment of the soil surrounding the pile, thereby reducing the effective temperature difference between the pile and the soil. This may lead to a gradual decline in heat exchange efficiency during subsequent cycles.

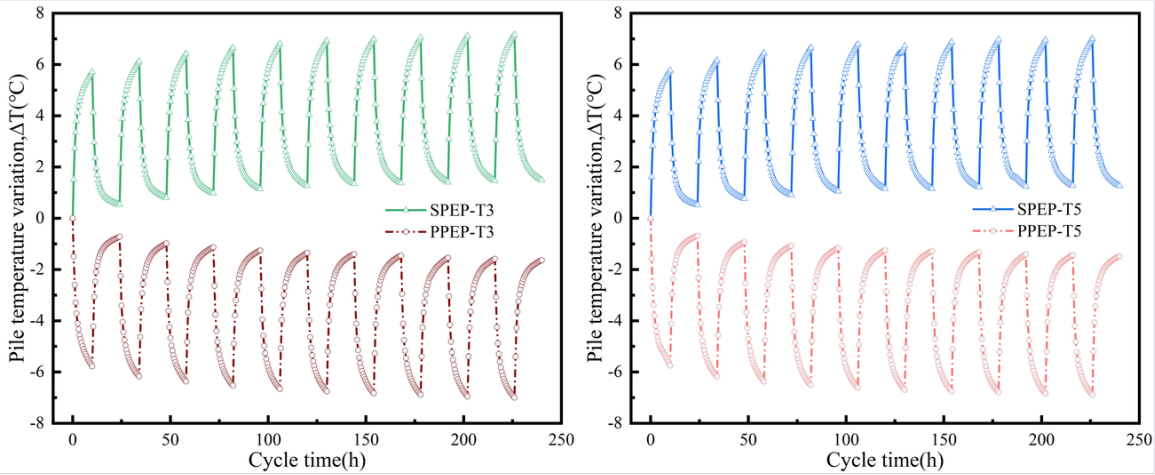

Figure 6. Temperature variations in the pile body over time.

A comparison of the amplitude of the temperature responses between SPEP and PPEP reveals a high degree of symmetry in absolute terms. In the first cycle, the difference in the T3 peak between the two was less than 0.07 °C; however, by the tenth cycle, the cumulative increase on the heating side (25.4%) was significantly higher than that on the cooling side (21.1%), with the peak difference widening to 0.17 °C. This asymmetry can be attributed to the temperature dependence of the soil's thermal properties, as well as the differential effects of heating expansion and cooling contraction on the thermal resistance at the pile-soil interface. In terms of the distribution of measurement points, the temperature response trends of T3 and T5 were highly consistent; however, both the peak and residual temperatures of T3 were slightly higher than those of T5 (the average peak difference over 10 cycles was 0.06 °C for SPEP and 0.05 °C for PPEP), reflecting the geometric characteristic that T3 is located at a radial position closer to the heat exchange pipe, resulting in a shorter heat conduction path.

3.2. Soil temperature

Figure 7 shows the radial soil temperature distribution at depth T3 for the SPEP. The peak temperature at the heat exchange pipe (approximately 0.15 m from the pile center) remained within 35–36 °C across all three cycles (H1 approx. 35.8 °C, H5 approx. 35.7 °C, H10 approx. 35.6 °C), indicating stable thermal resistance and heat transfer characteristics between the tube and surrounding soil. However, the temperature at the pile center showed significant thermal accumulation, rising from 21.4 °C in H1 to 25.6 °C in H10. This trend was also observed along the pile wall, suggesting that while soil dissipates heat after each cycle, residual heat causes a gradual rise in the temperature baseline for subsequent cycles. In the thermal influence zone, the temperature at 1D rose from 20.06 °C in H1 to 21.25 °C in H10, while the temperature at 2D increased to 20.34 °C, with minimal changes at 3D, indicating that the heat-affected zone expands but the rate of expansion slows in distant regions.

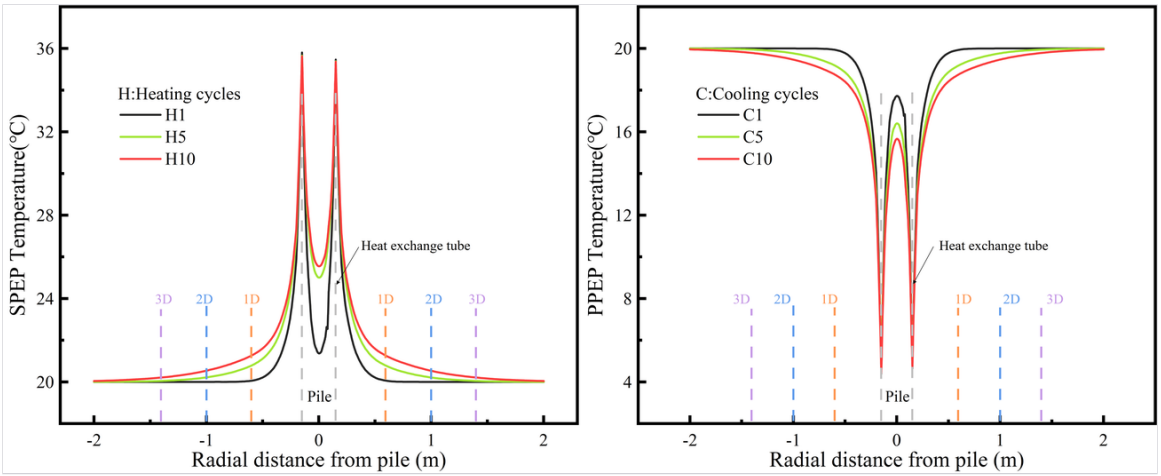

Figure 7. Radial temperature distribution in the soil (at depth T3).

Figure 7 also illustrates the radial temperature distribution for PPEP during cooling cycles at the same depth. The minimum temperature at the heat exchange tube was 4.4 °C in C1, 4.8 °C in C5, and 4.4 °C in C10, confirming the stability of heat exchange. The center temperature decreased from 17.7 °C in C1 to 15.6 °C in C10, a cumulative decrease of approximately 2.1 °C. Temperatures at the pile wall also decreased with each cycle, reflecting a cold accumulation effect similar to the heat accumulation in SPEP. At 1D, the temperature dropped from 19.9 °C in C1 to 18.8 °C in C10, and at 2D, it decreased by 0.3 °C. The temperature deviation at 3D remained minimal, indicating the cooling influence extends to 2D. Compared to SPEP, the far-field temperature disturbance in PPEP cooling is slightly higher, particularly at 1D, likely due to non-linear changes in soil thermal properties across different temperature ranges. Overall, the cumulative cycle effects are confined within the 2D range, offering valuable insight into the thermodynamic stability of the soil around energy piles during long-term operation.

Figure 8 shows the temperature contour plots of the pile cross-section for SPEP and PPEP at depth T3 at three typical time points: 10 h, 106 h, and 226 h. Under SPEP heating conditions, a high-temperature zone forms around the heat exchange pipe at 10 hours, reaching nearly 36 °C, while the rest of the pile remains near 20 °C. As time progresses to 106 h and 226 h, the high-temperature zone stabilizes, but heat gradually spreads into the pile and concrete, expanding the high-temperature region. The overall temperature of the pile increases, transitioning from dark blue to light blue. PCM aggregate particles within the pile show different temperature responses due to the endothermic phase change, acting as a buffer and reducing the temperature gradient compared to non-PCM regions. Under PPEP cooling conditions, the temperature field evolves symmetrically to the heating scenario. At 10 hours, a low-temperature zone forms near the heat exchange pipe, reaching approximately 4 °C, while the distal end remains close to 20 °C. Over time, the low-temperature zone expands, and the overall pile temperature decreases, transitioning from deep red to light red and orange. During cooling, PCM aggregate's exothermic phase change slightly increases its temperature, slowing heat transfer to the distant regions. Overall, the temperature distribution in the pile remains non-uniform, centered on the heat exchange tube. The PCM aggregate improves temperature uniformity to some extent, but its effect is limited by the volume fraction and spatial distribution density, especially in regions farther from the heat exchange pipe.

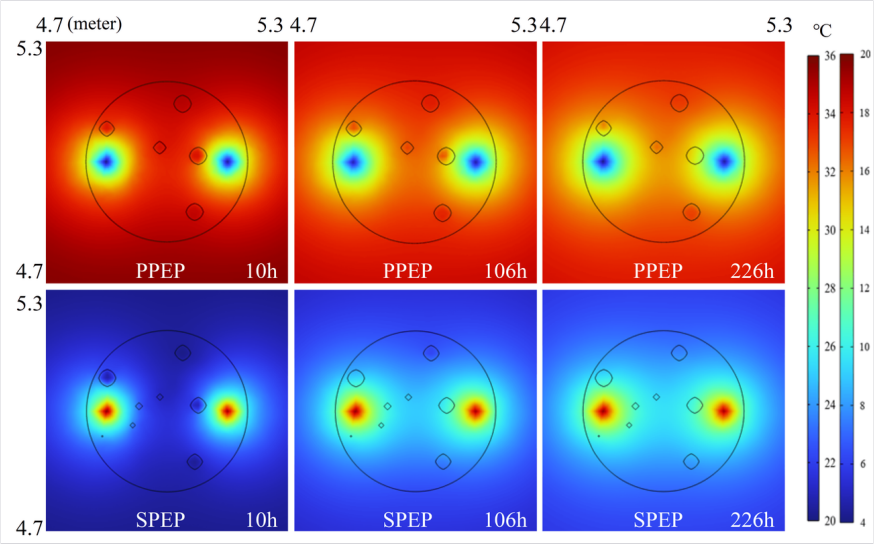

Figure 8. Cloud plot of the pile cross-section (at depth T3).

Figure 9 shows the temperature evolution over time for SPEP and PPEP at different radial distances on the T3 depth plane (T3, T8, T13, T18, increasing distance from the pile center). Under SPEP heating conditions, the temperature at T3 (closest to the pile) shows significant sawtooth-shaped fluctuations. During each heating cycle, the temperature rises sharply and drops during the recovery phase, but doesn't return to the previous cycle's starting point, forming an increasing baseline. The peak temperature at T3 rose from 25.71 °C in the first cycle to 27.17 °C in the tenth cycle, with a cumulative increase of 1.46 °C. The baseline temperature also rose from 20.53 °C to 21.48 °C, a cumulative shift of 1.48 °C, indicating irreversible heat accumulation in the surrounding soil. As the radial distance increased, the temperature response amplitude decayed, and time lag effects became more pronounced. At T8, the temperature rose by 1.33 °C, and at T13, only 0.56 °C, with nearly monotonic increases. At T18, the temperature rose by just 0.23 °C, indicating that thermal disturbances had dissipated. Under PPEP cooling conditions, temperature evolution is symmetrical. The minimum temperature at T3 during the first cooling cycle was 14.22 °C, dropping to 13.05 °C by the tenth cycle, a cumulative shift of 1.21 °C, slightly less than the SPEP heating condition. The baseline temperature at T3 decreased from 19.28 °C to 18.36 °C, with a cumulative deviation of 1.64 °C, indicating significant residual cooling capacity in the surrounding soil. At T8, temperatures dropped by 1.30 °C; at T13, 0.56 °C; and at T18, only 0.23 °C. The temperature rise in the far-field region was symmetrical between SPEP and PPEP conditions. Notably, the amplitude of temperature fluctuations and baseline drift at each point converged as the number of cycles increased. For example, at T3 in the SPEP scenario, the peak temperature increment between the 1st and 5th cycles was 1.10 °C, but only 0.36 °C between the 5th and 10th cycles. This indicates that the pile-soil heat exchange system is approaching dynamic thermal equilibrium, although a steady state has not been reached within 10 cycles, and the thermal environment around the pile continues to evolve.

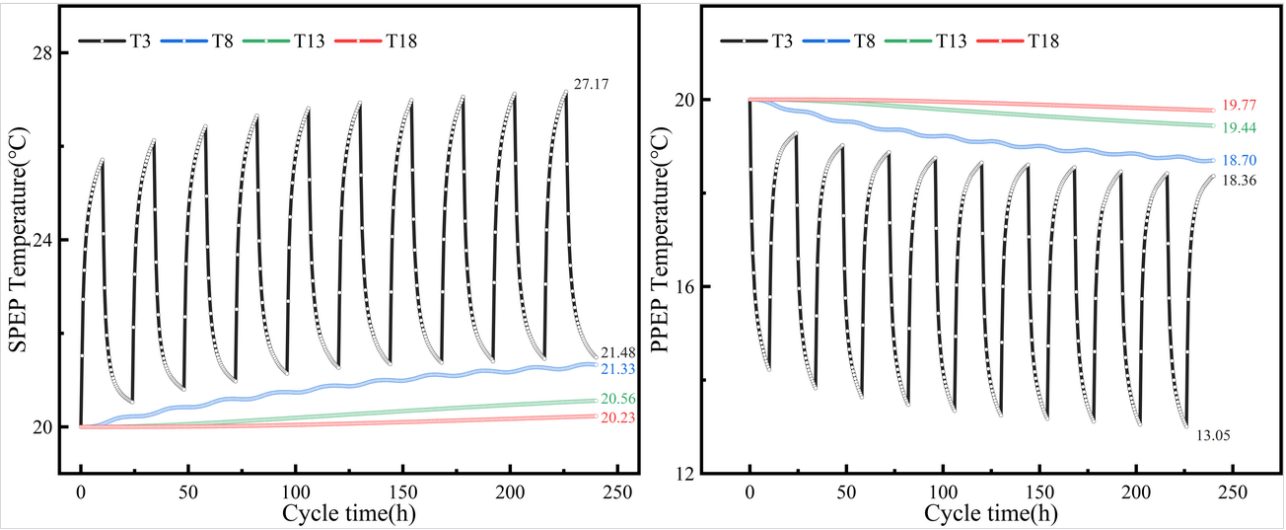

Figure 9. Soil temperature distribution over the course of the cycle.

3.3. Heat transfer efficiency

Equation 1 calculates the heat transfer efficiency per metre of the energy pile based on the difference between the inlet and outlet water temperatures; this efficiency provides an effective means of assessing the decline in heat transfer efficiency during the operation of the energy pile, as well as the efficiency of geothermal energy extraction during the final steady-state phase.

$$q = \frac{\rho \upsilon C_p (T_{out} - T_{in})}{L_1} \quad (1)$$

In the equation: q represents the heat transfer efficiency, W/m; ν represents the fluid flow rate, m^3/h; T_{out} and T_{in} represent the outlet and inlet temperatures of the heat exchange pipe, respectively, °C; L_1 represents the effective length of the pile, m.

Figure 10 illustrates the variation of heat transfer efficiency over time for the SPEP and PPEP operating conditions during the 1st, 5th and 10th thermal cycles. Data for each cycle are calculated from the first hour onwards to eliminate the influence of initial instability. Overall, both operating conditions exhibit similar temporal characteristics: heat transfer efficiency drops sharply at the beginning of each cycle before gradually stabilising. For the SPEP operating condition (heating phase), the initial peak values for each cycle are broadly comparable, but the steady-state heat transfer efficiency exhibits a decreasing trend as the number of cycles increases. It drops from 93.85 W/m in the first cycle to 87.43 W/m in the fifth cycle, and further to 81.30 W/m in the tenth cycle, representing a cumulative decline of approximately 13.4%. The PPEP operating condition (cooling phase) exhibited a similar decay pattern, with the absolute value of the steady-state heat transfer efficiency decreasing from 67.28 W/m in the first cycle to 59.43 W/m in the fifth cycle and 56.38 W/m in the tenth cycle, representing a cumulative decline of approximately 16.2%. It is worth noting that the rate of decline in heat exchange efficiency gradually slows as the number of cycles increases. Under SPEP conditions, the quasi-steady-state efficiency decreased by 6.42 W/m over the first five cycles, whereas it decreased by only 6.13 W/m over the subsequent five cycles. This trend is even more pronounced under PPEP conditions, with decreases of 7.85 W/m and 3.05 W/m in the corresponding intervals, respectively. The above phenomena indicate that, due to a thermal imbalance between the heating and cooling phases, progressive heat accumulation occurs in the soil surrounding the pile during cyclic operation. This leads to an increase in ground temperature, which in turn reduces the temperature gradient between the energy pile and the surrounding medium, resulting in a gradual decrease in heat transfer efficiency. However, the decreasing trend in the rate of decline also suggests

that, as the number of cycles increases, the energy pile–soil system gradually approaches a new state of thermal equilibrium. Furthermore, the absolute values of heat transfer efficiency for PPEP were lower than those for SPEP in all cycles, reflecting the inherent asymmetry in thermal response between heating and cooling modes under the current operating and geological conditions.

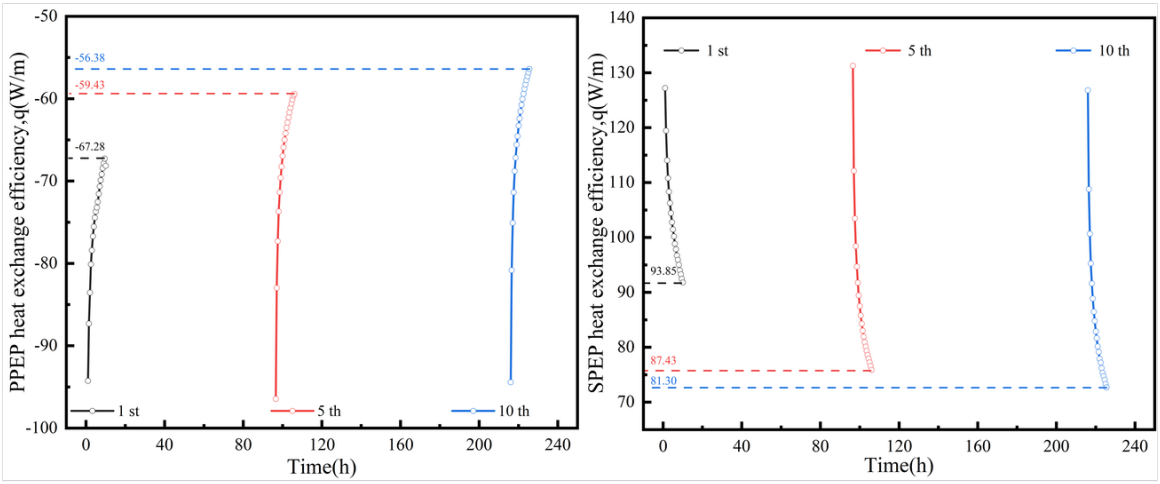

Figure 10. Variation of heat exchange efficiency with cycle time.

Equation 2 can be used to assess the relationship between the geothermal energy extraction capacity of a ground-source heat pump system and the electrical energy input. A higher coefficient of performance (COP) indicates that the ground-source heat pump system is more efficient at transferring heat.

$$COP = \frac{Q}{W_{sys}} \tag{2}$$

In the above equation, *COP* denotes the coefficient of performance of the ground-source heat pump system. *Q* represents the system's heat exchange power, W. W_{sys} represents the system's input power, 150 W.

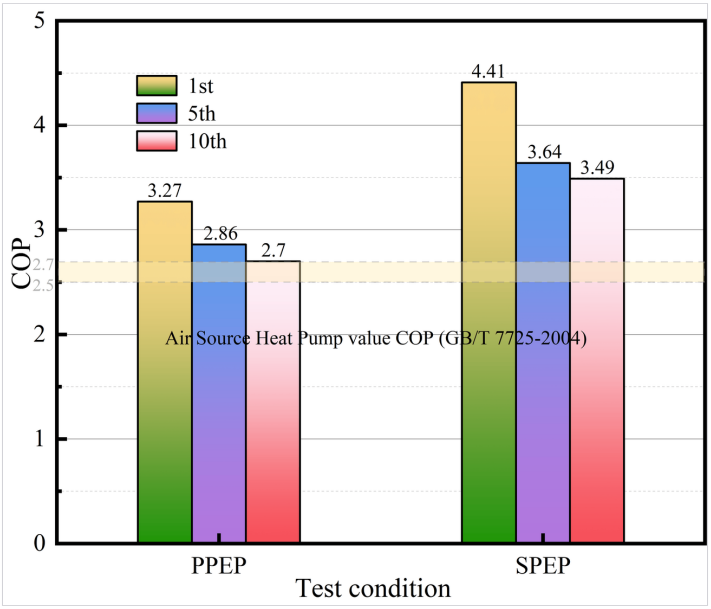

Figure 11. COP based on energy pile system.

Figure 11 compares the coefficient of performance (COP) for the SPEP and PPEP operating conditions during the 1st, 5th and 10th thermal cycles, with a constant system input power of 150 W. The results show that the COP for both operating conditions exhibits a downward trend as the number of cycles increases, but there are significant differences in the magnitude and rate of decline. The COP for the SPEP operating condition decreased from 4.41 in the first cycle to 3.64 in the fifth cycle, and further to 3.49 in the tenth cycle, representing a cumulative decline of approximately 20.9%. The rate of decline was relatively steep between the 1st and 5th cycles (0.77), whereas it narrowed significantly between the 5th and 10th cycles (0.15), indicating that system performance tends to stabilise after multiple cycles. Under PPEP conditions, the COP decreased from 3.27 in the first cycle to 2.86 in the fifth cycle, and further to 2.70 in the tenth cycle, representing a cumulative decline of approximately 17.4%. This also exhibits the characteristic of rapid initial decline followed by a slower rate of decline in the later stages. Across all operating conditions, the COP under SPEP remained consistently higher than that under PPEP. This is consistent with the conclusions of the aforementioned analysis of heat exchange efficiency and further confirms that the energy pile exhibits superior heat exchange capabilities in heating mode. Taking the reference COP values for air-source heat pumps (approximately 2.5–2.7) specified in the national standard GB/T 7725-2004 as a benchmark, the COP under SPEP conditions remained significantly higher than this benchmark even after the 10th cycle, whereas under PPEP conditions, the COP had already dropped to 2.70 by the 10th cycle, approaching the upper limit for air-source heat pumps. This indicates that as the number of cycles increases further, the economic advantages of the PPEP operating mode may gradually diminish. The aforementioned COP decline pattern essentially stems from the progressive thermal accumulation effect in the soil surrounding the pile during the cycling process. The thermal imbalance between the heating and cooling phases causes the ground temperature to gradually deviate from its initial state, weakening the temperature difference for heat transfer between the energy pile and the soil, thereby reducing the heat exchange output per unit of input power.

4. Conclusion

(1) The random aggregate method provides a physically more realistic representation of HSB-PCM distribution within the concrete matrix compared with conventional homogenisation models. By modelling each PCM particle as a discrete inclusion undergoing independent phase change based on local temperature.

(2) The PEP system exhibits progressive stabilization under cyclic loading. Depth-wise temperature gradients converged from 0.490–0.541 °C (1st cycle) to 0.257–0.344 °C (10th cycle). Despite recovery rates of 77–80% confirming the PCM buffering effect, residual temperatures at T3 reached 1.49 °C (SPEP) and −1.64 °C (PPEP), indicating an irreversible drift in the soil thermal environment.

(3) Efficiency declined by 13.4% (SPEP) and 16.2% (PPEP) over 10 cycles due to soil thermal accumulation. Crucially, the rate of decline decelerated: SPEP decreased by 6.42 W/m in the first five cycles versus 6.13 W/m in the latter five, suggesting the pile-soil system gradually approaches a new thermal equilibrium.

(4) Over 10 cycles, SPEP COP (4.41 to 3.49) remained well above the air-source heat pump benchmark (2.5–2.7), whereas PPEP COP (3.27 to 2.70) approached the benchmark's upper limit. This performance asymmetry suggests that the long-term economic advantage of cooling-mode PEP may diminish, necessitating seasonally balanced designs.

(5) The radial thermal influence of the energy pile is primarily confined within a range of twice the pile diameter (2D). At this distance, the cumulative temperature disturbance over 10 cycles remained below 0.34 °C for both operating conditions, while temperature deviations beyond 3D did not exceed 0.2 °C. These findings provide a quantitative basis for determining minimum pile spacing to avoid thermal interference in energy pile group configurations.

Declarations

Author contributions. Zhengheng Gan: Writing (original draft), Writing (review and editing). Mei Yin: Conceptualization, Funding acquisition. Shiqi Dou: Software. Hu Fan: Visualization. Chaokai Zhang: Methodology.

Funding. This research was funded by the National Natural Science Foundation of China(52678523) and the Postgraduate Research & Practice innovation Program of jiangsu Province (26CXJH0600).

Conflicts of interest. The authors declare that they have no known competing financial interests or personal relationships that could have appeared to influence the work reported in this paper.

Data availability. Data will be made available on request.

References

Adebayo, Philip; Beragama Jathunge, Charaka; Darbandi, Amirhossein; Fry, Nicholas; Shor, Roman; Mohamad, Abdulmajeed; Wemhöner, Carsten; Mwesigye, Aggrey (2024) 'Development, modeling, and optimization of ground source heat pump systems for cold climates: A comprehensive review', *Energy and Buildings*, 320, pp. 114646. Available at: https://doi.org/10.1016/j.enbuild.2024.114646

Angrisani, Giovanni; Entchev, Evgueniy; Roselli, Carlo; Sasso, Maurizio; Tariello, Francesco; Yaïci, Wahiba (2016) 'Dynamic simulation of a solar heating and cooling system for an office building located in Southern Italy', *Applied Thermal Engineering*, 103, pp. 377-390. Available at: https://doi.org/10.1016/j.applthermaleng.2016.04.094

Bourne-Webb, P.J.; Bodas Freitas, T.M. (2020) 'Thermally-activated piles and pile groups under monotonic and cyclic thermal loading–A review', *Renewable Energy*, 147, pp. 2572-2581. Available at: https://doi.org/10.1016/j.renene.2018.11.025

Cao, Ziming; Zhang, Guozhu; Liu, Yiping; Zhao, Xu; Li, Chenglin (2022) 'Influence of backfilling phase change material on thermal performance of precast high-strength concrete energy pile', *Renewable Energy*, 184, pp. 374-390. Available at: https://doi.org/10.1016/j.renene.2021.11.100

Chang, Hong; Gan, Zhengheng; Zhao, Huang; Li, Yunjie; Jiang, Haozhi; Wu, Xing; Zhao, Songying (2024) 'Thermo-mechanical behavior of steel pipe energy piles under thermal imbalance cycles', *Construction and Building Materials*, 447, pp. 138026. Available at: https://doi.org/10.1016/j.conbuildmat.2024.138026

Chang, Hong; Du, Yuan; Wu, Xing; Wang, Zhaoxuan; Jiang, Huicheng; Jiang, Sheng; Zhao, Songying; Gan, Zhengheng (2025) 'Effect of operating modes on graphite-based thermally enhanced heat exchanger', *International Communications in Heat and Mass Transfer*, 169, pp. 109561. Available at: https://doi.org/10.1016/j.icheatmasstransfer.2025.109561

Chang, Hong; Jiang, Huicheng; Du, Yuan; Li, Yunjie; Wu, Xing; Wang, Zhaoxuan; Jiang, Sheng; Gan, Zhengheng (2026a) 'Energy storage optimization of composite phase change material and fiber synergistically enhanced concrete: Numerical modeling and experiment', *Journal of Building Engineering*, 119, pp. 115292. Available at: https://doi.org/10.1016/j.jobe.2026.115292

Chang, Hong; Du, Yuan; Li, Yunjie; Wu, Xing; Jiang, Huicheng; Wang, Zhaoxuan; Su, Xiaoping; Gan, Zhengheng (2026b) 'Model test study of customized phase change materials for energy piles under multiple cooling cycles', *Applied Thermal Engineering*, 289, pp. 129806. Available at: https://doi.org/10.1016/j.applthermaleng.2026.129806

Chen, Kehao; Shen, Yang; Liu, Jiaxin; Wang, Chaoran; Han, Chanjuan (2024) 'Thermomechanical performance analysis of MicroPCM-enhanced energy pile concrete: A multiscale numerical study and formulation design implications', *Journal of Building Engineering*, 86, pp. 108791. Available at: https://doi.org/10.1016/j.jobe.2024.108791

Chen, Pengju; Wang, Chenglong; Bouazza, Abdelmalek; Guo, Yachen; Kong, Gangqiang; Ding, Xuanming (2025) 'Assessment of phase change material within hollow steel balls mixed with graphite powder-enhanced concrete for underground energy structures', *Journal of Energy Storage*, 120, pp. 116489. Available at: https://doi.org/10.1016/j.est.2025.116489

Gan, Zhengheng; Yin, Mei; Dou, Shiqi; Chang, Hong; Jiang, Huicheng (2025) 'Enhanced thermal performance of energy piles based on composite phase change material and random aggregate modelling', *Energy*, 341, pp. 139511. Available at: https://doi.org/10.1016/j.energy.2025.139511

Ghezellou, Amirmohammad; Keramati, Mohsen; Ghasemi-Fare, Omid (2024) 'Thermomechanical response of energy piles in dry sand under monotonic cooling with varying end-support conditions', *Journal of Energy Storage*, 82, pp. 110469. Available at: https://doi.org/10.1016/j.est.2024.110469

Han, Chanjuan; Yu, Xiong (Bill) (2020) 'Analyses of the thermo-hydro-mechanical responses of energy pile subjected to non-isothermal heat exchange condition', *Renewable Energy*, 157, pp. 150-163. Available at: https://doi.org/10.1016/j.renene.2020.04.118

Han, Chanjuan; Shen, Yang; Chen, Kehao; Gong, Cheng; Liu, Tianle; Qu, Bo (2022) 'Characteristics and energy performance of novel MicroPCM C50 energy pile in cooling mode', *Energy and Buildings*, 274, pp. 112442. Available at: https://doi.org/10.1016/j.enbuild.2022.112442

Hu, Chaoxin; Cui, Jie; Wang, Mingxuan; Zhang, Youliang; Luo, Jin; Li, Liangyong (2025) 'Optimizing the restoration performance of pipe energy piles using energy injection in winter mode: A numerical investigation', *Journal of Energy Storage*, 114, pp. 115807. Available at: https://doi.org/10.1016/j.est.2025.115807

Huang, Jingqi; Chen, Zhi; Xiao, Henglin; Xie, Huanzhen; Yu, Bin (2026) 'Study on the heat transfer performance of deep buried pipe energy pile with phase change backfill materials', *Geothermics*, 135, pp. 103539. Available at: https://doi.org/10.1016/j.geothermics.2025.103539

Kong, Ling-peng; Qiao, Lan; Xiao, Yun-yang; Li, Qing-wen (2019) 'A study on heat transfer characteristics and pile group influence of enhanced heat transfer energy piles', *Journal of Building Engineering*, 24, pp. 100768. Available at: https://doi.org/10.1016/j.jobe.2019.100768

Luu, Gia Trung; Wang, Chaoran; Han, Chanjuan (2025) 'Enhancing long-term viability of energy pile with heat sink systems in tropical monsoon climates: Implementation strategies and performance analysis', *Energy and Buildings*, 328, pp. 115119. Available at: https://doi.org/10.1016/j.enbuild.2024.115119

Morrone, Biagio; Coppola, Gaetano; Raucci, Vincenzo (2014) 'Energy and economic savings using geothermal heat pumps in different climates', *Energy Conversion and Management*, 88, pp. 189-198. Available at: https://doi.org/10.1016/j.enconman.2014.08.007

Mousa, M.M.; Bayomy, A.M.; Saghir, M.Z. (2022) 'Long-term performance investigation of a GSHP with actual size energy pile with PCM', *Applied Thermal Engineering*, 210, pp. 118381. Available at: https://doi.org/10.1016/j.applthermaleng.2022.118381

Mu, Jingyi; Feng, Yimeng; Yang, Dazhi; Yang, Guoming (2026) 'CMIP6 climate change and wind environment impacts on cold-region residential energy and thermal comfort: A case study of Harbin', *Energy for Sustainable Development*, 90, pp. 101885. Available at: https://doi.org/10.1016/j.esd.2025.101885

Ng, C.W.W.; Shi, C.; Gunawan, A.; Laloui, L.; Liu, H.L. (2015) 'Centrifuge modelling of heating effects on energy pile performance in saturated sand', *Canadian Geotechnical Journal*, 52(8), pp. 1045-1057. Available at: https://doi.org/10.1139/cgj-2014-0301

Reboli, Tommaso; Gini, Lorenzo; Mantelli, Luca; Traverso, Alberto (2025) 'Model predictive control of a phase-change-material thermal energy storage device at industrial relevant scale', *Energy Conversion and Management*, 346, pp. 120563. Available at: https://doi.org/10.1016/j.enconman.2025.120563

Song, Shaokun; Zhao, Tingting; Qiu, Feng; Zhu, Wanting; Chen, Taorui; Guo, Yi; Zhang, Yang; Wang, Yuqi; Feng, Rui; Liu, Yang; Xiong, Chuanxi; Zhou, Jian; Dong, Lijie (2019) 'Natural microtubule encapsulated phase change material with high thermal energy storage capacity', *Energy*, 172, pp. 1144-1150. Available at: https://doi.org/10.1016/j.energy.2019.02.052

Song, Huaibo; Pei, Huafu; Xu, Dongsheng; Cui, Chunyi (2020) 'Performance study of energy piles in different climatic conditions by using multi-sensor technologies', *Measurement*, 162, pp. 107875. Available at: https://doi.org/10.1016/j.measurement.2020.107875

Weng, Ling; Lin, Jian; Xu, Zeshui; Lu, Jing (2025) 'The trapezium cloud-based method with heterogeneous information for selecting phase change materials in the latent heat energy storage system', *Journal of Energy Storage*, 123, pp. 116649. Available at: https://doi.org/10.1016/j.est.2025.116649

Wu, D.; Liu, H.; Kong, G.; Li, C. (2019) 'Thermo-mechanical behavior of energy pile under different climatic conditions', *Acta Geotechnica*, 14(5), pp. 1495-1508. Available at: https://doi.org/10.1007/s11440-018-0731-9

Xia, Yang; Wu, Wenan; Yang, Yongtao; Fu, Xiaodong (2021) 'Mesoscopic study of concrete with random aggregate model using phase field method', *Construction and Building Materials*, 310, pp. 125199. Available at: https://doi.org/10.1016/j.conbuildmat.2021.125199

Yang, Weibo; Sun, Taofu; Zhang, Chaoyang; Wang, Feng (2023) 'Experimental and numerical investigations of thermo-mechanical behaviour of energy pile under cyclic temperature loads', *Energy*, 267, pp. 126516. Available at: https://doi.org/10.1016/j.energy.2022.126516

Yang, Weibo; Xia, Wenxin; Qiang, Yuhan; Wang, Feng (2025) 'Experimental and numerical investigations on thermo-mechanical behaviours of energy pile group with different seepage parameters', *Construction and Building Materials*, 472, pp. 140748. Available at: https://doi.org/10.1016/j.conbuildmat.2025.140748

Yin, Hang; Ying, Shicheng; Liu, Guangbin; Yang, Qichao; Zhao, Yuanyang; Li, Liansheng (2025) 'Energy, exergy, economic, and environmental analysis of waste heat source heat pump industrial steam generation system', *Energy Conversion and Management*, 330, pp. 119662. Available at: https://doi.org/10.1016/j.enconman.2025.119662

You, Tian; Zeng, Weitao (2023) 'Zoning operation of energy piles to alleviate the soil thermal imbalance of ground source heat pump systems', *Energy and Built Environment*, 4(1), pp. 57-63. Available at: https://doi.org/10.1016/j.enbenv.2021.08.001

Zhang, Yangkai; Sang, Guochen; Du, Xiaoyun; Cui, Xiaoling; Zhang, Lei; Zhu, Yiyun; Guo, Teng (2021) 'Development of a novel alkali-activated slag-based composite containing paraffin/ceramsite shape stabilized phase change material for thermal energy storage', *Construction and Building Materials*, 304, pp. 124594. Available at: https://doi.org/10.1016/j.conbuildmat.2021.124594

HOW TO CITE THIS PAPER

Gan, Z., Yin, M., Dou, S., Fan, H. and Zhang, C. (2026). Climatic Adaptability of Customized Phase Change Energy Piles Based on the Random Aggregate Method. In: *Proceedings of the 22nd International Conference on Sustainable Energy Technologies (SET2026)*, Kuala Lumpur, Malaysia, 13 to 15 August 2026. Caravel Press, pp. 11–26. ISBN 978-1-995850-00-9. ISSN 2978-4387. https://doi.org/10.65582/set.2026.002

COPYRIGHT AND LICENCE

© 2026 The Author(s). This is an open access paper distributed under the terms of the Creative Commons Attribution (CC BY 4.0) licence, which permits unrestricted use, distribution and reproduction in any medium, provided the original work is properly cited.

WSSET World Society of Sustainable Energy Technologies Organised by the World Society of Sustainable Energy Technologies. Published by Caravel Press.